IEEE Access
Multidisciplinary | Rapid Review | Open Access Journal

Received November 10, 2020, accepted December 10, 2020, date of publication December 25, 2020,
date of current version January 6, 2021.

Digital Object Identifier 10.1109/ACCESS.2020.3047517

A Fast and Accurate Method of Synthesizing X-Wave Launchers by Metallic Horns

SRĐAN PAKOVIĆ[1], NICOLA BARTOLOMEI[1], MARIO JUNIOR MENCAGLI[2], (Member, IEEE), MAURO ETTORRE[1], (Senior Member, IEEE), RONAN SAULEAU[1], (Fellow, IEEE), AND DAVID GONZÁLEZ-OVEJERO[1], (Senior Member, IEEE)

[1]CNRS, Institut d'Électronique et des Technologies du numéRique (IETR), UMR 6164, University of Rennes, F-35000 Rennes, France
[2]Department of Electrical and Computer Engineering, The University of North Carolina at Charlotte, Charlotte, NC 28223, USA

Corresponding author: Srđan Paković (srdan.pakovic@univ-rennes1.fr)

This work was supported in part by the European Union through the European Regional Development Fund (ERDF), and in part by the Ministry of Higher Education and Research, Brittany and Rennes Métropole, through the Contrat de plan État-Région (CPER) Project SOPHIE/STIC and Ondes. The work of Mario Junior Mencagli and David González-Ovejero was supported by the FACE Foundation through the Thomas Jefferson Fund.

ABSTRACT This paper presents a method for synthesizing metallic horns capable of radiating highly localized electromagnetic pulses, known as X-waves. The proposed method is based on a mode-matching framework for shaped horns. The aperture field distribution required to generate X-waves is synthesized by mode conversion. The near-field horns generated by this method are full-metal structures radiating X-waves in a wide range of frequencies with low dispersion. The obtained structures may be scaled to any frequency range, and they are particularly suited to millimeter and sub-millimeter wave applications. We validate the concept by presenting a horn capable of radiating X-waves over a 44% fractional bandwidth (FBW) with a 5° dispersion of the axicon angle. Capabilities and limitations of this design procedure and the synthesized launchers are demonstrated, discussed, and compared with other state-of-the-art solutions.

INDEX TERMS Bessel beams, mode-matching, near-field focusing, non-diffractive waves, X-waves.

I. INTRODUCTION

In past decades, Bessel beams have received large attention by the physics and engineering communities. Among their applications in optics and in microwave engineering, one finds medical imaging [1], wireless power transfer [2], and electron microscopy [3], to name a few. Ideal Bessel beams, which were introduced in 1987 by Durnin [4], are exact solutions of the Helmholtz equation that do not suffer from diffractive spreading while propagating. They are defined as follows

$$\Psi(\rho, \phi, z, t) = J_n(\chi\rho)e^{in\phi}e^{i(k_z z-\omega t)}, \tag{1}$$

where Ψ denotes a solution of the scalar Helmholtz wave equation, ω is the angular frequency, and (χ, k_z) are the radial and longitudinal components of the wave vector $\vec{k}$, respectively, such that $\left|\vec{k}\right|^2 = \chi^2 + k_z^2 = (\omega/c)^2$. In turn, $J_n(\chi\rho)$ stands for the standard Bessel function of the first kind and n-th order, with n an integer number. The variables ρ, ϕ and z are the cylindrical coordinates, with z being the assumed direction of propagation. Theoretically, ideal Bessel beams require infinite energy for their realization, namely, infinite radiating apertures. However, finite apertures can generate truncated Bessel beams which resist diffraction effects over a limited distance known as the "non-diffractive" range, limited by the axicon angle $\theta = \arctan(\chi/k_z)$.

In the literature, various methods have been reported for the generation of Bessel beams. In optics, some of the methods used include holography [5], axicon lenses [6], [7], and plasmonic metasurfaces [8]. In the microwave and millimeter-wave regimes, some of the adopted approaches encompass radial line slot antennas (RLSA) [9], [10], [11], leaky radial waveguides [12], [13], [14], metasurfaces [15], and loop antennas in a circular waveguide [16].

The polychromatic superposition of Bessel beams creates X-waves, which consist of electromagnetic pulses that resist diffraction and remain confined in both the transversal and longitudinal directions as they propagate up to a certain distance, after which they experience diffraction. Ideal X-waves are defined by the expression [17]

$$\chi(\rho, z, t) = \int_{-\infty}^{\infty} J_0[\chi(\omega)\rho]e^{-ik_z(\omega)z}e^{i\omega t}d\omega, \tag{2}$$

where J_0 is the Bessel function of the first kind and 0-th order. Some of the reported practical applications of X-waves

The associate editor coordinating the review of this manuscript and approving it for publication was Vittorio Degli-Esposti.

include secure short-range wireless communication [18] and biomedical ultrasound imaging [19].

Just like their monochromatic Bessel counterpart, the synthesis of ideal X-waves requires infinite apertures. In other terms, finite apertures can radiate truncated X-waves over limited frequency bands. We will refer to the finite frequency band in which truncated X-waves are generated as the operating frequency band, and to its ratio to the central frequency of the band as the fractional bandwidth (FBW). Unlike for Bessel beams, there exist only a few experimental demonstrations of X-wave generation in literature. This is due to inherent difficulties in realizing Bessel beam launchers with low-dispersive axicon angles θ over a wide frequency band. The first realization of X-waves was done in acoustics [20], followed by other proofs of concept in optics [21], [22].

The first experimental demonstration of X-waves in the microwave frequency range (from 19 to 29 GHz) was reported in 2018 [23]. The presented launcher consists of a CNC-milled dielectric lens surrounded by a copper tape fed by a coaxial cable. The launcher is capable of radiating X-waves over a 42% FBW with a 2° dispersion of the axicon angle θ. Despite these excellent characteristics, the use of dielectrics in [23] renders this realization lossy at higher frequencies. A similar demonstration of X-waves has been reported in [24], where the launcher uses a 3D printed dielectric metamaterial instead of the dielectric lens. This prototype can radiate X-waves over a 50% FBW with a 7° dispersion of the axicon angle θ. As in [23], the use of dielectrics can make such a solution lossy in the millimeter and sub-millimeter wave regimes. The use of a radial parallel-plate waveguide antenna was also proposed for generating X-waves and experimentally validated in [25]. The main drawback of [25] is the dispersive nature of radial launchers (24° for a 22% FBW). Capabilities of RLSA launchers based on Bessel and Hankel aperture distribution to radiate X-waves were theoretically analyzed in [26]. The drawback of [26] is, as in [25], the high dispersion of the axicon angle in RLSA launchers.

In this paper, we present a solution to generate X-waves by metallic horns. Metallic horns are a very common solution for transmitting radio waves due to their wide bandwidth, radiation characteristics, and simple construction and excitation. An overview of metallic horns and their applications, from their historical beginnings to current research activities, can be found in [27]. In previous decades, many techniques have been proposed to improve the performance of metallic horns. One of the most common approaches includes modifying the metallic profile of the horn by introducing corrugations [28], [29]. Some excellent characteristics of corrugated horns have been reported, such as dual-band operation [30], high Gaussicity and a very low sidelobe level (up to -60 dB) [31], large bandwidth [32], and dual-polarization [33].

To avoid the manufacturing issues of corrugated horns, Granet *et al.* proposed in 2004 smooth-walled spline-profiled metallic horns [34]. Such horns are designed by optimizing their profile to match the far-field to a specified radiation pattern. Excellent characteristics of spline-profiled horns have also been reported, such as low cross-polarization [35], multi-band operation [36], low sidelobe level [37], and high Gaussicity at THz frequencies [38], [39]. Performance of such antennas can be further improved by, for instance, integrating a dielectric lens [40], [41].

In this contribution, we optimize the shape of a smooth profile horn to generate X-waves in the near field. More precisely, the goal is to shape the profile to convert an axisymmetric mode at the input into an axisymmetric mode at the aperture capable of radiating X-waves. The design procedure is based on an ad-hoc mode-matching framework. Such horns are broadband, low-dispersive, do not require dielectrics or focusing elements to generate X-waves, and are scalable to any frequency range, making them particularly suited to millimeter and sub-millimeter wave applications [42]

The paper is organized as follows: Sections II and III present, respectively, the numerical formulation and the practical implementation of the proposed technique. Section IV presents an example of a transvere electric (*TE*) X-wave launcher with 44% FBW and 5° dispersion of the axicon angle generated by the proposed method. The capabilities and limitations of the presented procedure and related launchers are discussed in Section V and compared to other state-of-the-art launchers. Section VI demonstrates the capability of this technique to generate transverse magnetic (*TM*) X-wave launchers. To conclude, final remarks are reported in Section VII.

II. DESIGN CRITERIA

It has been shown in [43] that TE_{0n} and TM_{0n} modal field distributions in circular waveguides correspond to azimuthally and radially polarized truncated Bessel beams. Without loss of generality, in the following sections we will focus on TE_{0n} modal field distributions in circular waveguides. The proposed methodology can also be applied to TM_{0n} field distributions, as discussed in Section VI.

The non-diffractive range of truncated Bessel beams is limited by the axicon angle $\theta = \arctan(\chi/k_z)$ and given by the expression

$$z_{max} = a\sqrt{\left(\frac{k}{\chi}\right)^2 - 1}, \tag{3}$$

where a is the radius of the aperture and k is the magnitude of the wave vector $\vec{k}$. From (3), it is clear that larger non-diffractive ranges correspond to smaller transverse propagation constants/axicon angles and larger apertures, as skecthed in Fig. 1.

Therefore, once the radiating aperture has been fixed, the problem of designing Bessel beam launchers with large non-diffractive ranges reduces to synthesizing TE_{0n} modes on circular apertures with smaller values of the axicon angle θ. Additionally, for TE_{0n} modes $\chi = \chi_{0n} = x'_{0n}/a$, where x'_{0n} is the zero of the derivative of the Bessel function of the corresponding mode. It is thus clear that lower-order modes require smaller apertures for achieving the same non-diffractive distance compared to higher-order modes.

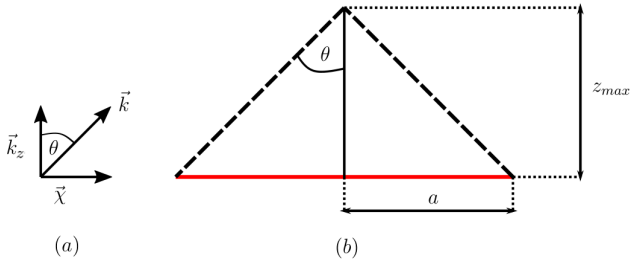

FIGURE 1. Graphic representation of the non-diffractive range (a) Decomposition of the wave vector $\vec{k}$, (b) Non-diffractive range defined by the aperture (red line) and the axicon angle θ.

Superposing truncated Bessel beams over a limited range of frequencies leads to the generation of truncated X-waves, as long as θ is low-dispersive. In [17], the criteria for synthesizing well-confined X-waves is defined by a "confinement factor", given by

$$C_{z,\rho} = \frac{j_{0,1}}{\pi m^2 \cos^2\theta \overline{\Delta\omega}} < 1, \tag{4}$$

where $j_{0,1} = 2.4048$ identifies the first zero of the J_0 function, $m = a/\lambda_0$ is the normalized aperture radius in terms of wavelengths and $\overline{\Delta\omega} = \Delta\omega/\omega_0$ is the fractional operative Bessel beams bandwidth. The distance up to which such truncated X-waves resist diffraction effects corresponds to the non-diffractive range z_{max} at the central frequency of the observed frequency band $\Delta\omega$.

To summarize, the problem of synthesizing X-waves reduces to synthesizing TE_{0n} modes on circular apertures sufficiently large and over a sufficiently wide frequency range to satisfy (7) with a low-dispersive axicon angle θ in the entire frequency band. For instance, one can verify using (7) that an aperture with a radius of $a = 3\lambda$ and an axicon angle of $\theta = 20°$ requires at least 10% of fractional bandwidth. We will use this criteria as a practical guideline for synthesizing X-wave launchers, as demonstrated in the following sections.

III. DESIGN PROCEDURE

For synthesizing a field distribution capable of radiating X-waves, we have resorted to a known property: an axisymmetric TE_{0n} mode at the junction of two circular waveguides of different radii will excite only the other axisymmetric TE_{0m} modes, with n and m being arbitrary integer numbers [44]. Applying this property, the design procedure consists in creating a structure which converts a TE_{01} mode at the input, which we assume we can generate correctly, to another TE_{0m} mode at the aperture, while satisfying the previously defined criteria for radiating X-waves. A simple way to obtain a circular TE_{0m} mode consists of a series of monotonically increasing constant waveguide sections, which we convert to a continuous profile.

To simplify and accelerate the design process, we developed an in-house mode-matching tool [44] for calculating the scattering matrix S, near-field, and far-field radiation of metallic horns with azimuthal symmetry. The tool approximates continuous antenna structures as a series of electrically short and concatenated cylindrical waveguides, with cylinder radii changing on each waveguide section. We choose the length of the cylindrical waveguide electrically small (typically less than $\lambda/10$) to assume that the resulting structure is continuous, as sketched in Fig. 2. Approximating the structure in such a way allows one to analyze it with a standard mode matching procedure [44]. We match the transverse field distribution at each discontinuity of the horn and cascade it section by section. This way, we can compute the aperture field distribution for a given profile, and consequentially the near and far-field distributions of the resulting structure. In this analysis, we assume that the structure includes a perfectly conducting infinite ground plane. Since the E-field vanishes on such a ground plane and is negligible beyond, we can assume that the E-field becomes zero beyond the radiating aperture. This modal approach is much faster than other full-wave methods (e. g. finite elements or finite integral technique [45]) and, despite the adopted approximations, the obtained results are in very good agreement with such methods.

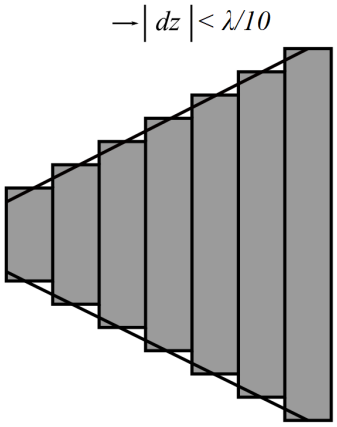

FIGURE 2. Approximation of a circular metallic continuous structure with a series of small depth cylinders.

In the following, we will assume that only the higher-order TE_{01} mode is present in the input circular waveguide. One can guarantee this behavior using well-known mode converters, e.g., [46]–[48], to transform the fundamental mode of a rectangular waveguide to a TE_{01} circular waveguide mode. The Marié converter in [46] offers excellent performance in terms of purity of the output TE_{01} mode, while being well-matched over a large band of frequencies. This mode converter is made of metal, allowing flexibility in terms of the operating frequency range. Inherent drawbacks of the Marié mode converter are its electrical length, which can be a potential problem if used at lower frequencies, and its geometrical complexity. However, it has been shown that these limitations can be conveniently overcome by using additive manufacturing [48].

The targeted TE_{0n} field distribution can be chosen arbitrarily. As mentioned before, larger non-diffractive ranges can be achieved by using either larger apertures or by smaller transverse propagation constants. Therefore, it is generally convenient to design an electrically smaller antenna and target the field distribution of a lower-order mode (TE_{01} or TE_{02})

on its aperture. In particular, we optimize the depths and radii of multiple waveguide sections to couple the aperture field distribution to the field distribution of a TE_{01} or a TE_{02} mode. More precisely, we require $S_{21} > 0.92$ between the incident TE_{01} mode and the targeted output TE_{01} or TE_{02} mode at each frequency point (85% of power coupling). Such constraint proved to be sufficient for the effective radiation of Bessel beams/X-waves. The second goal of the optimization was to match the synthesized horn to the input TE_{01} mode. The targeted value of the input reflection coefficient is $S_{11} \leq -15$ dB. We also impose a design constraint on the Marié mode converter in the optimization routine, requiring that the output radius of the mode converter (input of the horn) guarantees the TE_{02} mode in cutoff, so only the TE_{01} mode can propagate. Due to the large number of optimization variables, we used the interior-point method in the optimization procedure to minimize the following cost function

$$F_c = \sum_f S_{21}^{error}(f) + W \sum_f S_{11}^{error}(f), \tag{5}$$

where $S_{21}^{error}(f)$ and $S_{11}^{error}(f)$ are distances between the achieved and targeted S parameters (L1 norm) at the frequency point f and W is the weight coefficient used to control the priority of the factors. The polynomial complexity of the interior point method makes it a more appropriate choice for this type of large-scale non-linear optimization problems in comparison with other similar methods (e. g. simplex).

The initial structure has a conical profile with prescribed length and input and output radii. The input radius is initially fixed to be smaller than $r_{TE_{02}}$, where $r_{TE_{02}}$ is the smallest radius that supports a propagating TE_{02} mode at the highest in-band frequency. In turn, the output radius a is calculated using (3) to provide the targeted non-diffractive range z_{max}. The initial length of the horn is related to the targeted non-diffractive range and possible starting values are provided in Section V. Then, the conical profile is approximated as a series of monotonically increasing waveguide sections. Each waveguide section is defined by 2 optimization variables: its depth and radius. Typically, the number of used sections N should be greater than L/λ_0, where L is the length of the horn. The optimization procedure then modifies the structure by tuning the $2N$ optimization variables until the value of the cost function (5) is zero. One iteration cycle of the optimization process consists in the following consecutive steps:

- Generate the profile of the structure by defining depths and radii of cascading waveguide sections,
- Calculate the S_{11} of the structure for the TE_{01} mode at the input,
- Calculate the coupling between the incident TE_{01} mode and the targeted output TE_{01} or TE_{02} modes,
- Calculate the value of the cost function using (5),
- If the goal value of the cost function is not satisfied ($F_c > 0$), the profile of the structure is modified by changing the $2N$ variables according to the used optimization algorithm and the cycle is repeated. If the goal value of the cost function is satisfied ($F_c = 0$), the optimization procedure stops.

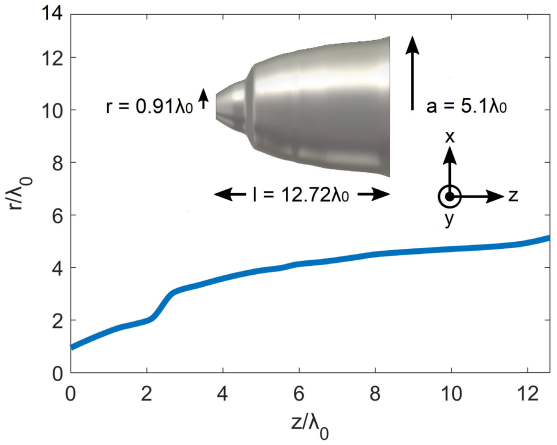

FIGURE 3. Dimensions of the realized profile in terms of wavelenght at the central frequency. Inset: Synthesized metal horn.

IV. NUMERICAL VALIDATION

The design procedure was validated by synthesizing a TE_{02} launcher capable of radiating Bessel beams over a 44% of fractional bandwidth. Fig. 3 presents the exact dimensions of the realized profile and the synthesized metal horn. Since the launchers designed by the procedure are full-metal structures, they may be scaled to any frequency range. Therefore, all results in this and the following sections will be in terms of free-space wavelengths λ_0 at the central frequency f_0 of the operating frequency range.

The input radius of the launcher is $r_0 = 0.91\lambda_0$, which satisfies the aforementioned design constraint of the Marié mode converter, requiring that the TE_{02} mode is in cutoff in the entire frequency range. The radius of the aperture is $a \approx 5.1\lambda_0$, which corresponds to $z_{max} \approx 23\lambda_0$ of non-diffractive range at the central frequency and 12° axicon angle θ at the central frequency with 5° dispersion in the operating bandwidth. The total length of the launcher is around $12.72\lambda_0$, and consists of 20 waveguide sections, with depths varying between 0.36 and $2.18\lambda_0$, which we convert to a continuous profile shown in of Fig. 3. This number of sections proved to be sufficient in this particular case. The used optimization procedure was the one described in Section III, with total optimization time being around 10 minutes. The optimization was performed on an Intel Xeon 2.6 GHz dual-core CPU with 128 GB RAM. The confinement factor of the launcher (7) is around 0.08, allowing the radiation of well-confined pulses. The widths of the generated pulse in transversal and longitudinal directions, which correspond to the null-to-null distance of the amplitude profile over the axes, are $S_\rho = 3.72\lambda_0$ and $S_z = 4.7\lambda_0$, respectively. The pulse widths were evaluated using following expressions [17]

$$S_\rho = \frac{2j_{0,1}c}{\omega_0 \sin\theta}, \tag{6}$$

$$S_z = \frac{4\pi c}{\Delta\omega \cos\theta}. \tag{7}$$

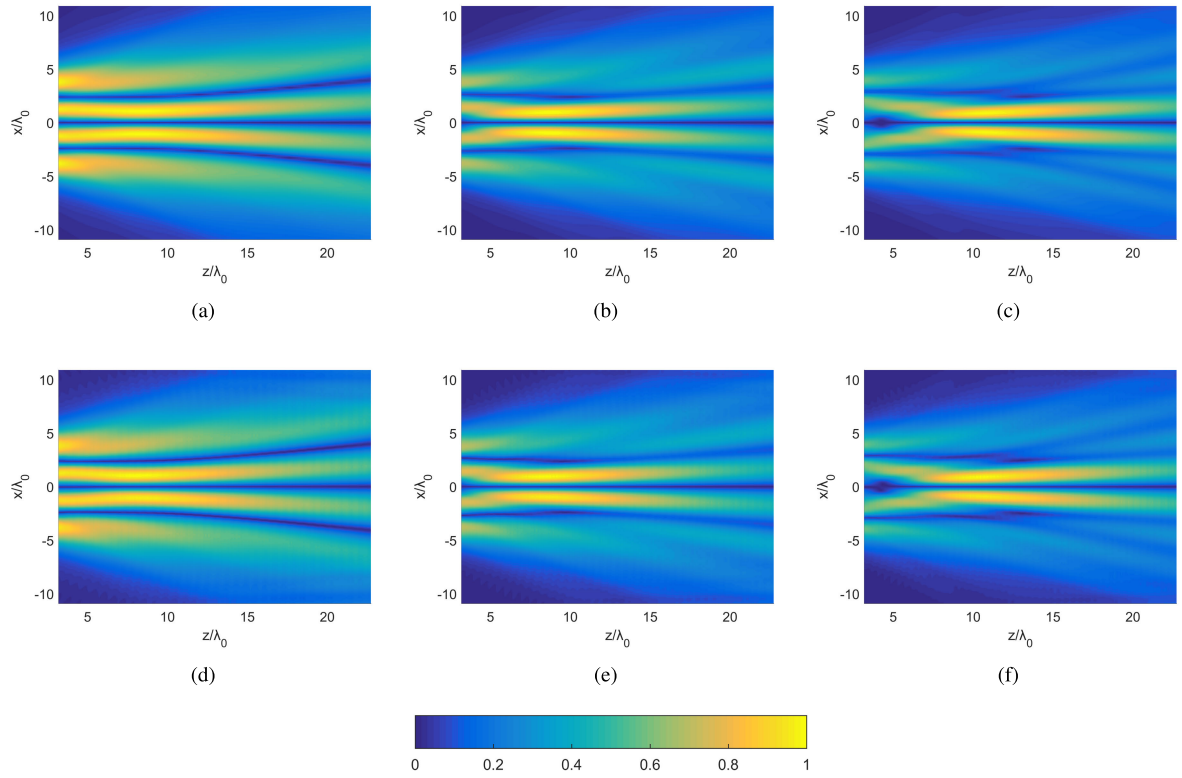

FIGURE 4. Calculated (a)-(c) and simulated (CST) (d)-(f) normalized E_y in the $x0z$ plane normalized to the wavelength at the central frequency within the non-diffractive range at (a) and (d) $f = 0.78f_0$, (b) and (e) $f = f_0$, (c) and (f) $f = 1.22f_0$.

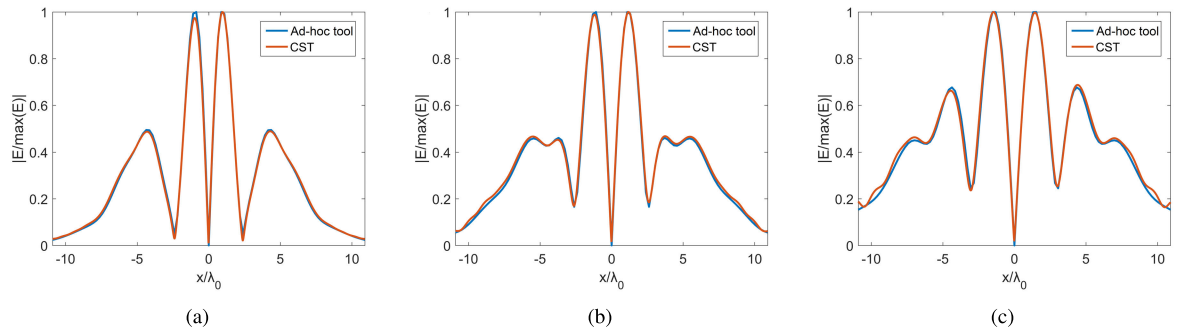

FIGURE 5. Normalized E_y along the x-axis at the central frequency at (a) $z = 9.2\lambda_0$, (b) $z = 13.8\lambda_0$ and (c) $z = 18.4\lambda_0$.

Finally, the S_{11} of the launcher is below -20 dB in the entire frequency range.

Next, we compare the performance of the X-wave launcher with full-wave simulations. First, we demonstrate the non-diffractive behavior of the structure. Fig. 4 presents the absolute value of the y component of the electric field (E_y) in the $x0z$ plane at three frequency points corresponding to the central frequency f_0 and the edges of the operating band, $0.78f_0$ and $1.22f_0$. The results in Figs. 4 (a)-(c) have been obtained with our mode-matching tool, while those in Figs. 4 (d)-(f) are CST Microwave Studio results [45]. The edges of the operating band correspond to frequency points in which the required coupling to the TE_{02} mode is not satisfied and the resulting radiated field distributions do not resemble Bessel beams anymore. Fig. 5 presents a comparison of the E_y along the x-axis at 9.2, 13.8, and $18.4\lambda_0$ above the aperture of the launcher at the central frequency. Figs. 4 and 5 demonstrate the non-diffractive behavior of the launcher in the prescribed range of frequencies. The excellent agreement between the results obtained with our numerical tool and CST's time domain solver in Fig. 5 validates the tool. Fig. 6 presents the instantaneous intensity of the pulse (i. e. longitudinal component of the H-field), confirming the capability of the launcher to radiate well-confined X-waves and thus also validating the design procedure.

V. PERFORMANCE GUIDELINES

In order to determine the capabilities and limitations of the mode-converting procedure, we have synthesized X-wave launchers with TE_{01} and TE_{02} aperture field distributions.

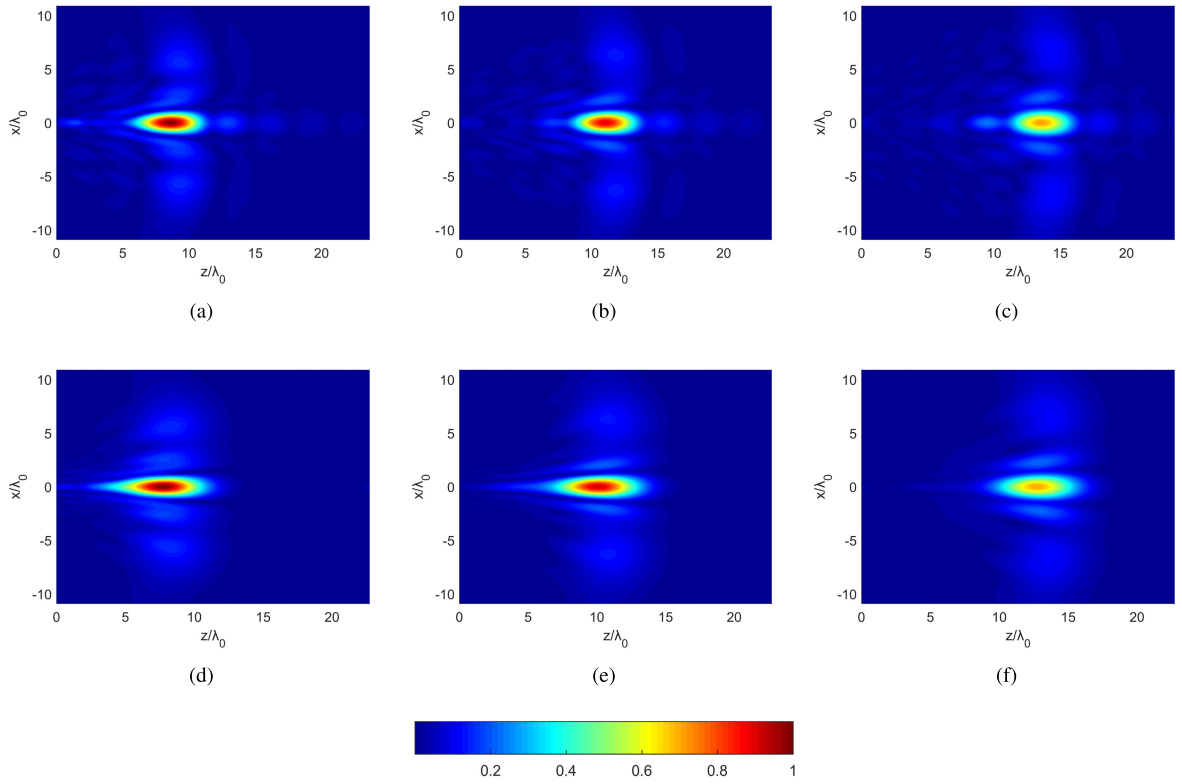

FIGURE 6. Calculated (a)-(c) and simulated (CST) (d)-(f) normalized instantaneous intensity of H_z in the $x0z$ plane normalized to the wavelength at the central frequency within the non-diffractive range at (a) and (d) $t = t_{max}$, (b) and (e) $t = t_{max} + 3/f_0$, (c) and (f) $t = t_{max} + 6/f_0$. t_{max} is the moment in time in which the intensity of the pulse is at its maximum value. The video from which (a)-(c) were extracted can be seen in the supplementary material of the paper.

We have considered specified values of non-diffractive range and a set of FBW for the synthesized launchers, while the input radius is fixed to support the propagation of a TE_{01} mode. In particular, we synthesized launchers with non-diffractive ranges spanning from 6 to 60 λ_0 with 11, 22, 33, and 44% FBW (with the same central frequency), with a fixed input radius $r_0 = 0.91\lambda_0$. The 44% FBW corresponds to the maximum value which we were able to achieve using the proposed optimization procedure. Since we are interested in determining the limits of this design technique, we modified the optimization routine to force the synthesized launchers to be as short as possible. We repeated the optimization routine several times for every specified value of the non-diffractive range to find the corresponding minimal length of the launcher, and the obtained values are displayed in Fig. 7.

From Fig. 7, one can note some important properties of the mode-converting procedure. Firstly, it is clear that to achieve longer non-diffractive ranges for the generated Bessel beams/X-waves, longer launchers are required. A peculiar property appears from Fig. 7: the ratio between the non-diffractive range and the minimal length of the launcher capable of radiating such a beam is almost linear. Longer launchers are also required to generate Bessel beams in a larger frequency band. Additionally, we can achieve the same non-diffractive range of the generated beam with a significantly smaller launcher by synthesizing a lower-order TE_{0n}

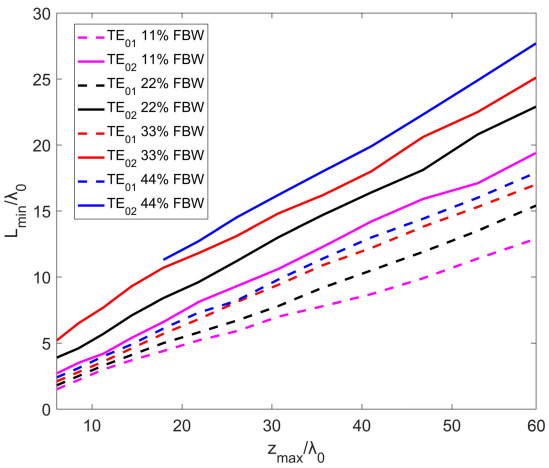

FIGURE 7. Ratio between the non-diffractive range and the minimal length of the launcher required for its generation in terms of wavelenght at the central frequency.

mode field distribution at the aperture. Finally, we were not able to achieve sufficient coupling to the TE_{02} for lower values of the non-diffractive range for 44% of FBW. This is most likely because the corresponding aperture radii become closer to the cutoff of the TE_{02} mode at the lower end of the frequency band, making it difficult to achieve the sufficient coupling to the TE_{02} mode without distorting field distributions at the higher end of the band.

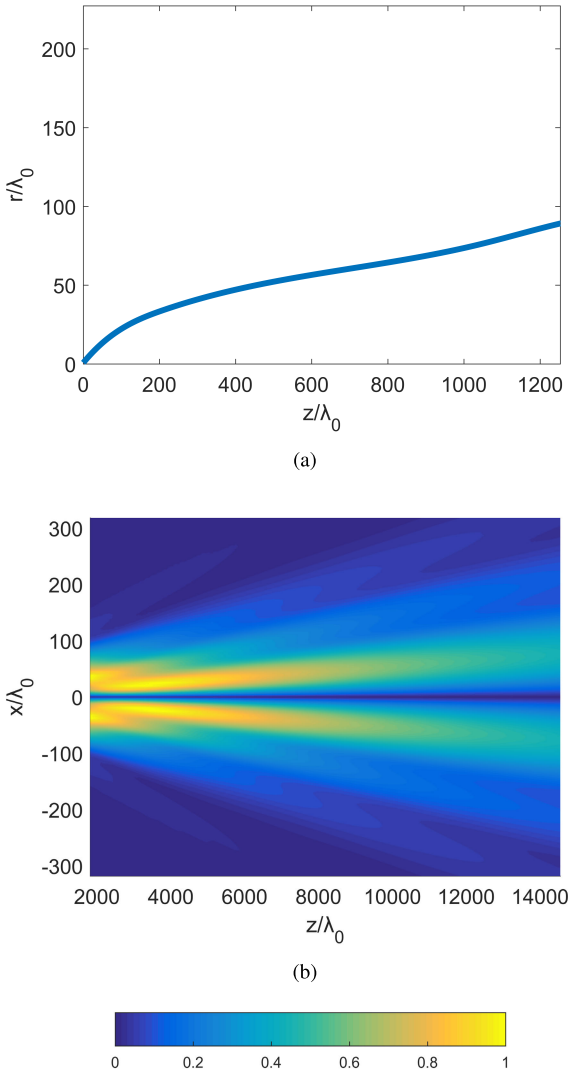

FIGURE 8. Long-range Bessel beam launcher. (a) Exact dimensions of the profile capable of radiating a long-range Bessel beam in terms of wavelength. (b) Normalized E_y of the launcher in the $x0z$ plane normalized to the wavelength within the non-diffractive range.

Notwithstanding this limitation, the results in Fig. 7 can be readily used to define the starting profile for the optimization in Section III. Moreover, these results demonstrate that the procedure is flexible in terms of the operating frequency band and also in terms of performances of the generated launchers. One can also note that, other than the trade-off between the size of the launcher and the achieved non-diffractive range, the method has no particular limitations in terms of the achievable non-diffractive range of the generated Bessel beam/X-wave.

To validate this claim, we synthesized a launcher capable of radiating a Bessel beam with the TE_{01} field distribution at the aperture with a $13000\lambda_0$ of non-diffractive range ($k_\rho/k = 0.0068$) at a single frequency point. Fig. 8 presents the exact dimensions of the profile and its E_y field distribution in the $x0z$ plane. In this particular case, the computational process was too demanding to apply the procedure on a range of frequencies, since the length of the launcher is around $1250\lambda_0$ and its radius is around $90\lambda_0$. However, based on previous results, we can assume that, other than computational issues, there should be no particular difficulties in synthesizing an X-wave launcher with such and even larger non-diffractive ranges. It is worth noting that structures of this size cannot be analyzed using other full-wave methods with available computational resources. It is also clear that the fabrication of such a device can only be attempted for quite short wavelengths.

TABLE 1. Tabular comparison of X-wave launchers.

Launcher	[23]	[24]	[25]	[26]	This work
FBW	42%	50%	22%	33%	44%
Aperture radius	$8\lambda_0$	$4\lambda_0$	$9\lambda_0$	$16\lambda_0$	$5.1\lambda_0$
z_{max}	$24\lambda_0$	$6.7\lambda_0$	$22\lambda_0$	$180\lambda_0$	$23\lambda_0$
θ at f_0	20°	14°	19°	5°	12°
Dispersion of θ	2°	7°	24°	35°	5°
Low-profile	No	No	Yes	Yes	No
Full-metal	No	No	No	No	Yes

To provide a better understanding of the capabilities of the proposed launchers, we compare the capabilities of the launcher from Section III to other solutions used to generate X-waves: a dielectric lens filling a standard horn antenna [23], a dielectric metamaterial filling a standard horn antenna [24], a radial parallel-plate waveguide antenna [25], and RLSA launchers [26]. Solutions [23] and [24] show good behavior in terms of FBW and the dispersion of the axicon angle θ. More precisely [23] has a 42% of FBW and 2° dispersion of θ, and [24] has a 50% of FBW and 7° dispersion of θ. On the other hand, the advantage of [25] and [26] is that the launchers are low-profile structures. However, their drawback is the dispersive nature of radial launchers, particularly [25] has a 24° dispersion of θ in 22% of FBW, and [26] has a 35° dispersion of θ in 33% of FBW.

In comparison with the other solutions, horns generated by our approach show good performance in terms of FBW and dispersion of θ (the horn given in Section IV has 44% of FBW with 5° of dispersion). Unlike other solutions, the generated horns are full-metal structures, overcoming the problems related to dielectric lenses at higher frequencies. Table 1 presents a comparison of the performance of the aforementioned launchers, as presented in the literature. The main drawback of our procedure is that the resulting structure (a cascade of the Marié mode converter and the horn) can be considered electrically large, especially if longer non-diffractive ranges are required. Although this might pose a size issue if the launchers are used at lower frequencies, the converter in [47] can help to render the TE_{01} launcher more compact.

VI. GENERATING TM X-WAVES

Finally, we discuss the capability of the described procedure to synthesize *TM* X-wave launchers. Intuitively, one may assume that the problem for *TM* X-wave launchers is identical to the problem for *TE* X-wave launchers: synthesizing

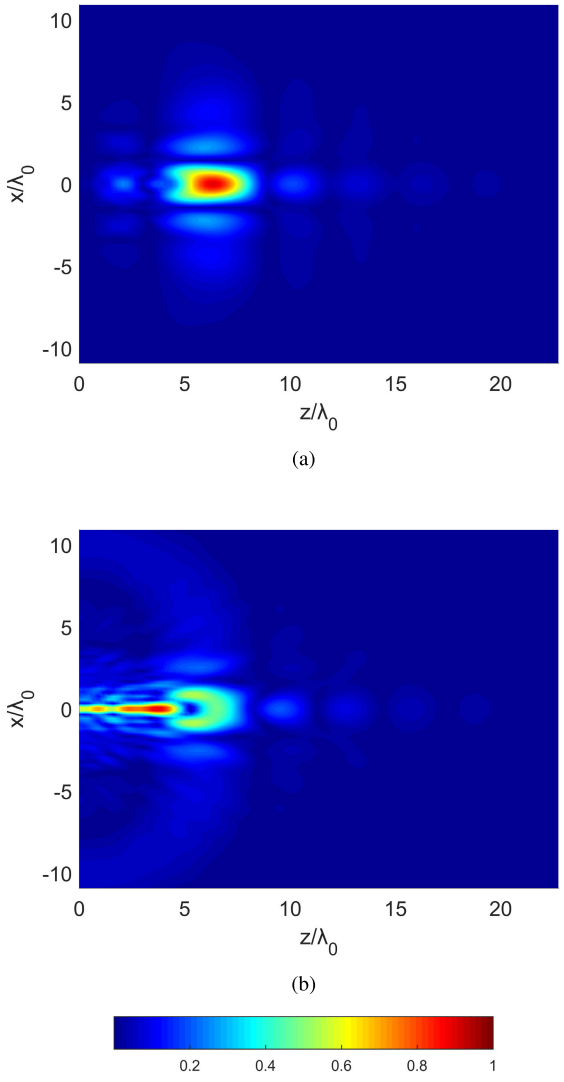

FIGURE 9. Distortion of a TM X-wave generated by a metallic horn antenna. (a) Normalized instantaneous intensity of H_z in the $x0z$ plane normalized to the wavelength at the central frequency of a TE X-wave with 44% of FBW within the non-diffractive range (b) Normalized instantaneous intensity of E_z along the $x0z$ plane normalized to the wavelength at the central frequency of a TM X-wave with 44% of FBW within the non-diffractive range in the same time slot t. The videos from which the pictures were extracted can be seen in the supplementary material of the paper.

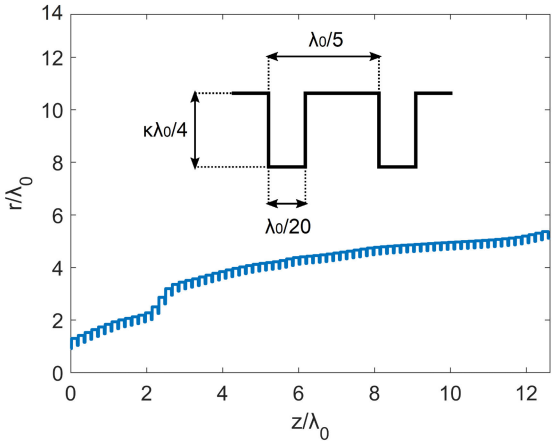

FIGURE 10. Corrugated profile of the TM_{02} launcher. Inset: Dimensions of the used corrugations in terms of wavelength. κ corresponds to the correction factor found in [29].

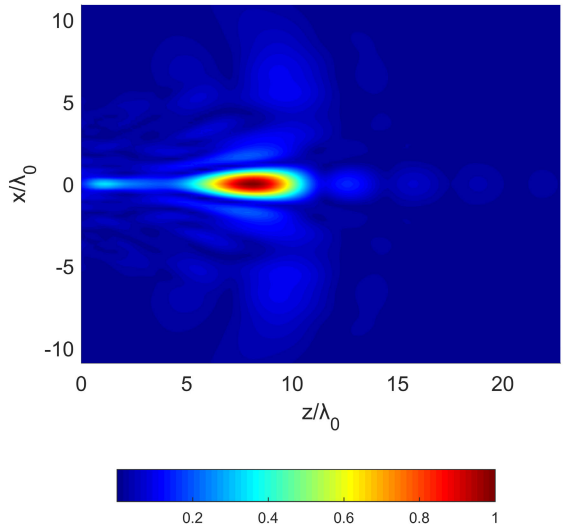

FIGURE 11. Calculated normalized instantaneous intensity of E_z along the $x0z$ plane normalized to the wavelength at the central frequency for a horn antenna with PMC boundaries within the non-diffractive range in $t = t_{max}$. The video from which the picture was extracted can be seen in the supplementary material of the paper.

metal horns with aperture field distributions matching TM_{0n} modes of circular waveguides in a range of frequencies so that (7) is satisfied. However, this is not the case. The resulting radiated field distribution of such an aperture distribution indeed resembles X-wave distributions discussed in previous sections. On the other hand, it is heavily distorted compared to *TE* X-waves, as sketched in Fig. 9. This is most likely because TM_{0n} E field distributions in waveguides have much stronger edge components, resulting in high diffraction.

It is well-known that modal field distributions in metal waveguides and perfect magnetic conductor (PMC) waveguides are dual: field distributions of *TE* modes in metal waveguides match the *TM* field distributions in PMC, and vice versa. For instance, we can use the same horns used for synthesizing *TE* X-waves, with PMC replacing the metal walls of the horn, and feed them with, for instance, a TM_{01} mode using the mode-converter presented in Section IV-A of [49]. For demonstration purposes, we replaced the metal walls of the horn radiating a TE_{02} X-wave from Section IV with corrugations to simulate PMC and fed the structure with a TM_{01} mode. Corrugations were designed according to [29] and the realized corrugated profile and normalized dimensions of these corrugations are shown in Fig. 10.

The expected performance of the *TM* launcher designed with an ideal PMC is identical to the performance of the *TE* launcher. However, since we use corrugations instead of an ideal PMC, small aberrations are expected. Fig. 11 presents the instantaneous intensity of the E_z in a time slot t_{max} in which the intensity of the pulse is at its maximum value. Comparing Fig. 11 to Fig. 6(d) it is evident that

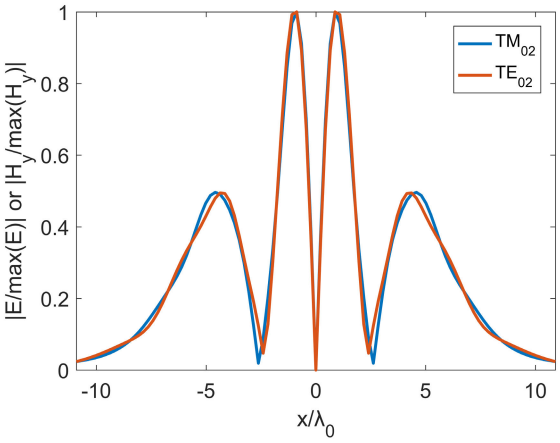

FIGURE 12. Comparison of the normalized E_y component of the TM_{02} launcher with the normalized H_y component of the TE_{02} launcher at $z = 9.1\lambda_0$.

the performance of the two launchers is nearly identical. In Fig. 12, by duality, we compare the E_z field profile of the TM_{02} launcher to the H_z field profile of the TE_{02} launcher along the x-axis $9.1\lambda_0$ above the aperture at a single frequency point. The excellent agreement of the profiles verifies that *TM* X-wave launchers synthesized by replacing the metal walls of *TE* X-wave launchers with PMC indeed have identical performance as their *TE* counterparts.

VII. CONCLUSION

In this paper, a novel method for synthesizing X-wave launchers by circular metallic horns has been presented. X-waves are radiated by an axisymmetric *TE* (or *TM*) field distribution on an electrically large aperture. The method has been implemented using an ad-hoc tool based on mode-matching framework. Launchers generated by the design procedure are full-metal horns, that present a low dispersion over a wide frequency range (more than 40% of FBW). We presented an example of a horn with 5° of dispersion of the axicon angle θ in a 44% of FBW. We have also demonstrated that the procedure can synthetize Bessel launchers with arbitrary non-diffractive ranges. In particular, we proposed a Bessel beam launcher of 13000λ of non-diffractive range. Moreover, we have shown that the ratio between the non-diffractive range of the beam and the minimal length of the launcher capable of radiating such a beam is almost linear. The designed launchers do not require dielectric material or focusing elements to radiate X-waves and are also scalable at any frequency, making them particularly suited to the millimeter and submillimeter wave regimes. The proposed method and generated tool pave the way for many practical applications of X-waves in the submillimeter bands, such as imaging and near-field wireless communications.

REFERENCES

[1] J. Lu and J. Greenleaf, "Diffraction-limited beams and their applications for ultrasonic imaging and tissue characterization," *Proc. SPIE*, vol. 1733, pp. 92–119, Nov. 1992.
[2] J. D. Heebl, M. Ettorre, and A. Grbic, "Wireless links in the radiative near field via bessel beams," *Phys. Rev. A, Gen. Phys.*, vol. 6, no. 3, Sep. 2016, Art. no. 034018.
[3] V. Grillo, J. Harris, G. C. Gazzadi, R. Balboni, E. Mafakheri, M. R. Dennis, S. Frabboni, R. W. Boyd, and E. Karimi, "Generation and application of bessel beams in electron microscopy," *Ultramicroscopy*, vol. 166, pp. 48–60, Jul. 2016.
[4] J. Durnin, "Exact solutions for nondiffracting beams. I. The scalar theory," *J. Opt. Soc. Amer. A, Opt. Image Sci.*, vol. 4, no. 4, pp. 651–654, Apr. 1987.
[5] J. Turunen, A. Vasara, and A. T. Friberg, "Holographic generation of diffraction-free beams," *Appl. Opt.*, vol. 27, no. 19, pp. 3959–3962, 1988.
[6] J. Durnin, J. J. Miceli, Jr., and J. H. Eberly, "Diffraction-free beams," *Phys. Rev. Lett.*, vol. 58, pp. 1499–1501, Apr. 1987.
[7] J. Arlt and K. Dholakia, "Generation of high-order bessel beams by use of an axicon," *Opt. Commun.*, vol. 177, nos. 1–6, pp. 297–301, Apr. 2000.
[8] F. Aieta, P. Genevet, M. A. Kats, N. Yu, R. Blanchard, Z. Gaburro, and F. Capasso, "Aberration-free ultrathin flat lenses and axicons at telecom wavelengths based on plasmonic metasurfaces," *Nano Lett.*, vol. 12, no. 9, pp. 4932–4936, Aug. 2012.
[9] A. Mazzinghi, M. Balma, D. Devona, G. Guarnieri, G. Mauriello, M. Albani, and A. Freni, "Large depth of field pseudo-bessel beam generation with a RLSA antenna," *IEEE Trans. Antennas Propag.*, vol. 62, no. 8, pp. 3911–3919, Aug. 2014.
[10] M. Albani, S. C. Pavone, M. Casaletti, and M. Ettorre, "Generation of non-diffractive Bessel beams by inward cylindrical traveling wave aperture distributions," *Opt. Exp.*, vol. 22, no. 15, pp. 18354–18364, Jul. 2014.
[11] S. C. Pavone, M. Ettorre, M. Casaletti, and M. Albani, "Transverse circular-polarized Bessel beam generation by inward cylindrical aperture distribution," *Opt. Exp.*, vol. 24, no. 10, pp. 11103–11111, 2016.
[12] M. Ettorre and A. Grbic, "Generation of propagating bessel beams using leaky-wave modes," *IEEE Trans. Antennas Propag.*, vol. 60, no. 8, pp. 3605–3613, Aug. 2012.
[13] M. Ettorre, S. M. Rudolph, and A. Grbic, "Generation of propagating bessel beams using leaky-wave modes: Experimental validation," *IEEE Trans. Antennas Propag.*, vol. 60, no. 6, pp. 2645–2653, Jun. 2012.
[14] P. Lu, D. Voyer, A. Breard, J. Huillery, B. Allard, X. Lin-Shi, and X.-S. Yang, "Design of TE-polarized bessel antenna in microwave range using leaky-wave modes," *IEEE Trans. Antennas Propag.*, vol. 66, no. 1, pp. 32–41, Jan. 2018.
[15] C. Pfeiffer and A. Grbic, "Controlling vector bessel beams with metasurfaces," *Phys. Rev. A, Gen. Phys.*, vol. 2, no. 4, Oct. 2014, Art. no. 044012.
[16] M. A. Salem, A. H. Kamel, and E. Niver, "Microwave bessel beams generation using guided modes," *IEEE Trans. Antennas Propag.*, vol. 59, no. 6, pp. 2241–2247, Jun. 2011.
[17] W. Fuscaldo, S. C. Pavone, G. Valerio, A. Galli, M. Albani, and M. Ettorre, "Analysis of limited-diffractive and limited-dispersive X-waves generated by finite radial waveguides," *J. Appl. Phys.*, vol. 119, no. 19, May 2016, Art. no. 194903.
[18] J.-Y. Lu and S. He, "Optical X wave communications," *Opt. Commun.*, vol. 161, nos. 4–6, pp. 187–192, Mar. 1999.
[19] J.-Y. Lu, H. Zou, and J. F. Greenleaf, "Biomedical ultrasound beam forming," *Ultrasound Med. Biol.*, vol. 20, no. 5, pp. 403–428, Jan. 1994.
[20] J.-Y. Lu and J. F. Greenleaf, "Experimental verification of nondiffracting X waves," *IEEE Trans. Ultrason., Ferroelectr., Freq. Control*, vol. 39, no. 3, pp. 441–446, May 1992.
[21] H. Sõnajalg, M. Rätsep, and P. Saari, "Demonstration of the Bessel-X pulse propagating with strong lateral and longitudinal localization in a dispersive medium," *Opt. Lett.*, vol. 22, no. 5, pp. 310–312, 1997.
[22] P. Saari and K. Reivelt, "Evidence of X-shaped propagation-invariant localized light waves," *Phys. Rev. Lett.*, vol. 79, no. 21, p. 4135, Nov. 1997.
[23] N. Chiotellis, V. Mendez, S. M. Rudolph, and A. Grbic, "Experimental demonstration of highly localized pulses (X waves) at microwave frequencies," *Phys. Rev. B, Condens. Matter*, vol. 97, no. 8, Feb. 2018, Art. no. 085136.
[24] N. Chiotellis, S. Zhang, Y. C. Vardaxoglou, and A. Grbic, "X wave radiator implemented with 3-D printed metamaterials," *IEEE Trans. Antennas Propag.*, vol. 68, no. 7, pp. 5478–5486, Jul. 2020.
[25] D. Comite, W. Fuscaldo, S. K. Podilchak, V. G.-G. Buendía, P. D. H. Re, P. Baccarelli, P. Burghignoli, and A. Galli, "Microwave generation of X-waves by means of a planar leaky-wave antenna," *Appl. Phys. Lett.*, vol. 113, Oct. 2018, Art. no. 114102.

[26] S. C. Pavone, A. Mazzinghi, A. Freni, and M. Albani, "Comparison between broadband Bessem beam launchers based on either Bessel or Hankel aperture distribution for millimeter wave short pulse generation," *Opt. Exp.*, vol. 25, no. 16, pp. 19548–19560, 2017.

[27] E. Lier, D. H. Werner, and T. S. Bird, "The evolution from metal horns to metahorns: The development of EM horns from their inception to the present day," *IEEE Antennas Propag. Mag.*, vol. 61, no. 4, pp. 6–18, Aug. 2019.

[28] P. J. B. Clarricoats and A. D. Olver, *Corrugated Horns for Microwave Antennas* (IEE Electromagnetic Waves Series), vol. 18. London, U.K.: Peter Peregrinus, 1984.

[29] C. Granet and G. L. James, "Design of corrugated horns: A primer," *IEEE Antennas Propag. Mag.*, vol. 47, no. 2, pp. 76–84, Apr. 2005.

[30] O. Sotoudeh, P.-S. Kildal, P. Ingvarson, and S. P. Skobelev, "Single- and dual-band multimode hard horn antennas with partly corrugated walls," *IEEE Trans. Antennas Propag.*, vol. 54, no. 2, pp. 330–339, Feb. 2006.

[31] J. E. McKay, D. A. Robertson, P. J. Speirs, R. I. Hunter, R. J. Wylde, and G. M. Smith, "Compact corrugated feedhorns with high Gaussian coupling efficiency and -60 dB sidelobes," *IEEE Trans. Antennas Propag.*, vol. 64, no. 6, pp. 2518–2522, Jun. 2016.

[32] J. Teniente, R. Gonzalo, and C. Del-Rio, "Ultra-wide band corrugated Gaussian profiled horn antenna design," *IEEE Microw. Wireless Compon. Lett.*, vol. 12, no. 1, pp. 20–21, Jan. 2002.

[33] S. Manshari, S. Koziel, and L. Leifsson, "Compact dual-polarized corrugated horn antenna for satellite communications," *IEEE Trans. Antennas Propag.*, vol. 68, no. 7, pp. 5122–5129, Jul. 2020.

[34] C. Granet, G. L. James, R. Bolton, and G. Moorey, "A smooth-walled spline-profile horn as an alternative to the corrugated horn for wide band millimeter-wave applications," *IEEE Trans. Antennas Propag.*, vol. 52, no. 3, pp. 848–854, Mar. 2004.

[35] H. Deguchi, M. Tsuji, and H. Shigesawa, "Compact low-cross-polarization horn antennas with serpentine-shaped taper," *IEEE Trans. Antennas Propag.*, vol. 52, no. 10, pp. 2510–2516, Oct. 2004.

[36] C. Granet and G. L. James, "Optimized spline-profile smooth-walled triband 20/30/44-GHz horns," *IEEE Antennas Wireless Propag. Lett.*, vol. 6, pp. 492–494, Nov. 2007.

[37] J. Wang, Y. Yao, J. Yu, and X. Chen, "Design of novel tanh/linear dual profiled smooth horn with low sidelobes," *Electron. Lett.*, vol. 53, no. 6, pp. 371–373, Mar. 2017.

[38] A. Hammar, Y. Karandikar, P. Forsberg, A. Emrich, and J. Stake, "A 340 GHz high gaussicity smooth spline horn antenna for the STEAMR instrument," in *Proc. IEEE Antennas Propag. Soc. Int. Symp. (APSURSI)*, Jul. 2014, pp. 649–650.

[39] D. A. Montofre, R. Molina, A. Khudchenko, R. Hesper, A. M. Baryshev, N. Reyes, and F. P. Mena, "High-performance smooth-walled horn antennas for THz frequency range: Design and evaluation," *IEEE Trans. THz Sci. Technol.*, vol. 9, no. 6, pp. 587–597, Nov. 2019.

[40] A. Rolland, R. Sauleau, and L. Le Coq, "Flat-shaped dielectric lens antenna for 60-GHz applications," *IEEE Trans. Antennas Propag.*, vol. 59, no. 11, pp. 4041–4048, Nov. 2011.

[41] A. Rolland, N. T. Nguyen, R. Sauleau, C. Person, and L. Le Coq, "Smooth-walled light-weight ka-band shaped horn antennas in metallized foam," *IEEE Trans. Antennas Propag.*, vol. 60, no. 3, pp. 1245–1251, Mar. 2012.

[42] G. Chattopadhyay, M. Alonso-delPino, N. Chahat, D. GonzÃĺlez-Ovejero, C. Lee, and T. Reck, "Terahertz antennas and feeds," in *Aperture Antennas for Millimeter and Sub-Millimeter Wave Applications*, A. Boriskin and R. Sauleau, Eds. Cham, Switzerland: Springer, 2017.

[43] Z. Bouchal and M. Olivík, "Non-diffractive vector bessel beams," *J. Mod. Opt.*, vol. 42, no. 8, pp. 1555–1566, Aug. 1995.

[44] G. Conciauro, M. Gugilelmi, and R. Sorrentino, *Advanced Modal Analysis*. New York, NY, USA: Wiley, 2000.

[45] *CST Microwave Studio*, CST Amer., Anaheim, CA, USA, 2016.

[46] S. S. Saad, J. B. Davies, and O. J. Davies, "Analysis and design of a circular TE01 mode transducer," *IEE J. Microw. Opt. Acoust.*, vol. 1, no. 2, pp. 58–62, Jan. 1977.

[47] C.-F. Yu and T.-H. Chang, "High-performance circular TEHigh-performance circular TE_{01}-mode converter 01-mode converter," *IEEE Trans. Microw. Theory Techn.*, vol. 53, no. 12, pp. 3794–3798, Dec. 2005.

[48] M. Gonzalez-Calvo, J. R. Montejo-Garai, J. A. Ruiz-Cruz, and J. M. Rebollar, "Additive manufacturing of a high-performance *Q*-band circular TE01 mode flared-type transducer," *IEEE Microw. Wireless Compon. Lett.*, vol. 29, no. 9, pp. 577–579, Sep. 2019.

[49] D. Gonzalez-Ovejero, N. Chahat, R. Sauleau, G. Chattopadhyay, S. Maci, and M. Ettorre, "Additive manufactured metal-only modulated metasurface antennas," *IEEE Trans. Antennas Propag.*, vol. 66, no. 11, pp. 6106–6114, Nov. 2018.

SRĐAN PAKOVIĆ received the B.S. and M.S. degrees in electrical engineering from the Univerzitet u Beogradu, Elektrotehnički fakultet, Belgrade, Serbia, in 2017. He is currently pursuing the Ph.D. degree in electronics with the Institut d'Électronique et des Technologies du numéRique (IETR), Rennes, France. His research interests include non-diffractive waves, near-field focusing, wireless power transfer, and computational electromagnetics.

NICOLA BARTOLOMEI received the B.Sc. degree and the M.Sc. degree *(cum laude)* in electronic engineering and the Ph.D. degree in telecommunication engineering from the University of Florence, in 2010, 2013, and 2017, respectively.

In 2016, he was a Visiting Student with Tsinghua University, Beijing, China, working on traveling wave slot antennas and transmitarrays. From May 2017 to February 2020, he was with the Institut d'Electronique et des Technologies du numéRique (IETR), University of Rennes 1, Rennes, France, as a Postdoctoral Fellow in a framework founded by Thales Alenia Space working on quasi-optical lenses for space applications. He is currently serving as an Antenna Engineer with Wave-Up, S.r.l, Siena, Italy, involved in Research and Development activities on beam scanning circularly polarized metasurface antennas. His research interests include numerical methods for scattering and antenna problems, periodic structures, and slot array design.

MARIO JUNIOR MENCAGLI (Member, IEEE) received the B.Sc. and M.Sc. degrees *(cum laude)* in telecommunications engineering from the University of Siena, Italy, in 2008 and 2013, respectively, and the Ph.D. degree *(cum laude)* in electromagnetics from the University of Siena, Italy, in 2016, under the supervision of Prof. S. Maci.

In 2014, he spent few months as a Visiting Ph.D. Student with Thales Research and Technology, Paris, France, where he was involved with characterization and testing of optically reconfigurable transmission lines based on checkerboard metasurfaces. From January 2017 to July 2019, he was a Postdoctoral Researcher with the Prof. Nader Engheta's Group, University of Pennsylvania, Philadelphia, PA, USA. Since August 2019, he has been an Assistant Professor with the Department of Electrical and Computer Engineering, The University of North Carolina, Charlotte, NC, USA. He organized a special session about low- and high-dimensional metamaterials at EuCAP 2020. He has given invited talks in highly ranked universities and institutions. He has been working on reconfigurable metasurface, periodic structures, RF circuits, numerical methods for electromagnetic problems, high-frequency techniques for electromagnetic scattering, metamaterials for both microwave and optical regimes, transformation optics, metatronic, filter at optical and UV frequencies, analog computing, and time-varying metamaterials.

Dr. Mencagli was granted with a three-year scholarship from Thales Research and Technology, in 2013. He was also a recipient of the Best Thesis Award of XXIX cycle of the Ph.D. Program in Information Engineering and Sciences at the University of Siena in 2018. This distinction is awarded by Springer Theses, which publishes a new book series with the selected Ph.D. Theses.

MAURO ETTORRE (Senior Member, IEEE) received the Laurea degree *(summa cum laude)* in electrical engineering and the Ph.D. degree in electromagnetics from the University of Siena, Italy, in 2004 and 2008, respectively.

Part of his Ph.D. work was developed at The Netherlands Organization for Applied Scientific Research (TNO), The Hague, The Netherlands, where he later worked as an Antenna Researcher. From 2008 to 2010, he was a Postdoctoral Fellow with the Institut d'Electronique et de Télécommunications de Rennes (IETR), University of Rennes 1, France. In 2010 and 2016, he was a Visiting Scholar with the Radiation Laboratory, Department of Electrical Engineering and Computer Science, University of Michigan, Ann Arbor, MI, USA. Since October 2010, he has been a Research Scientist with the Centre National de la Recherche Scientifique (CNRS), IETR. In 2014, he assumed responsibilities for the multi-beam antenna activity for satellite applications in the joint laboratory between IETR and Thales Alenia Space, France. In 2015, he was an Invited Professor with the Tokyo Institute of Technology (TIT), Japan. Since 2016, he has been the Secretary of the French National Committee for Scientific Research, Section 08 (micro- and nanotechnologies, photonics, and electromagnetism), CNRS, Paris, France. His research interests include the analysis and design of leaky-wave antennas, periodic structures, millimeter-wave antennas, non-diffractive radiation and localized waves, near-field focusing techniques, and wireless power transfer systems.

Dr. Ettorre was a member of the Best Paper Award selection committee for the IEEE Transactions on Terahertz Science and Technology, in 2017, 2018, and 2019. He received the Young Antenna Engineer Prize at the 2008 ESA Antenna Workshop in the Netherlands, the Innovation Award at 2018 ESA Antenna Workshop, The Netherlands, and the Best Paper Award in Electromagnetics and Antenna Theory at the 2018 European Conference on Antennas and Propagation (EuCAP), London, U.K. Since 2017, he has also been an Associate Editor of the IEEE Transactions on Antennas and Propagation.

RONAN SAULEAU (Fellow, IEEE) received the degree in electrical engineering and radio communications from the Institut National des Sciences Appliquées, Rennes, France, in 1995, the Agrégation degree from the Ecole Normale Supérieure de Cachan, France, in 1996, and the Ph.D. degree in signal processing and telecommunications and the Habilitation à Diriger des Recherches degree from the University of Rennes 1, France, in 1999 and 2005, respectively.

He was an Assistant Professor and an Associate Professor with the University of Rennes 1, from September 2000 to November 2005, and from December 2005 to October 2009, respectively, where he has been appointed as a Full Professor, since November 2009. He was a Co-Director of the research Department Antenna and Microwave Devices, IETR, and the Deputy Director of IETR from 2012 to 2016. He is currently the Director of IETR. He has been involved in more than 60 research projects at the national and European levels and has co-supervised 23 Postdoctoral Fellows, 44 Ph.D. students, and 50 master's students. He has received 17 patents and is the author or coauthor of more than 250 journal articles and 510 publications in international conferences and workshops. He has shared the responsibility of the research activities on antennas at IETR in 2010 and 2011. His current research interests include numerical modeling (mainly FDTD), millimeter-wave printed and reconfigurable (MEMS) antennas, substrate integrated waveguide antennas, lens-based focusing devices, periodic and non-periodic structures (electromagnetic bandgap materials, metamaterials, reflectarrays, and transmitarrays), and biological effects of millimeter waves.

Dr. Sauleau received the 2004 ISAP Conference Young Researcher Scientist Fellowship, Japan, and the first Young Researcher Prize, Brittany, France, in 2001, for his research work on gain-enhanced Fabry–Perot antennas. In September 2007, he was elevated to a Junior member of the Institut Universitaire de France. He was awarded the Bronze medal by CNRS in 2008 and the Silver Medal in 2020. He was a co-recipient of several international conference awards with some of his students (International School of BioEM 2005, BEMS'2006, MRRS'2008, E-MRS'2011, BEMS'2011, IMS'2012, Antem'2012, BioEM'2015, and EuCAP'2019). He served as a Guest Editor for the IEEE Antennas Propagate. Special Issue on Antennas and Propagation at mm and sub mm waves. He served as a National Delegate for several EU COST actions. He has served as a National Delegate for EurAAP and as a member for the board of Director of EurAAP from 2013 to 2018.

DAVID GONZÁLEZ-OVEJERO (Senior Member, IEEE) was born in Gandía, Spain, in 1982. He received the M.S. degree in telecommunication engineering from the Universidad Politécnica de Valencia, Valencia, Spain, in 2005, and the Ph.D. degree in electrical engineering from the Université catholique de Louvain, Louvain-la-Neuve, Belgium, in 2012.

From 2012 to 2014, he was a Research Associate with the University of Siena, Siena, Italy. In 2014, he joined the Jet Propulsion Laboratory, California Institute of Technology, Pasadena, CA, USA, where he was a Marie Curie Postdoctoral Fellow. Since 2016, he has been a Tenured Researcher with the French National Center for Scientific Research, Institut d'Electronique et de Télécommunications de Rennes, Rennes, France. He was a recipient of a Marie Curie International Outgoing Fellowship from the European Commission 2013, the Sergei A. Schelkunoff Transactions Prize Paper Award from the IEEE Antennas and Propagation Society in 2016, and the Best Paper Award in Antenna Design and Applications at the 11th European Conference on Antennas and Propagation in 2017. Since 2019, he has been an Associate Editor of the IEEE Transactions on Antennas and Propagation and the IEEE Transactions on Terahertz Science and Technology.